IEEE Access
Multidisciplinary | Rapid Review | Open Access Journal

Received January 10, 2020, accepted January 21, 2020, date of publication January 27, 2020, date of current version February 10, 2020.

Digital Object Identifier 10.1109/ACCESS.2020.2969806

A Hybrid Fuzzy Clustering Approach for the Recognition and Visualization of MRI Images of Parkinson's Disease

YO-PING HUANG[1,2], (Fellow, IEEE), PRITPAL SINGH[1], AND HUNG-CHOU KUO[3]

[1]Department of Electrical Engineering, National Taipei University of Technology, Taipei 10608, Taiwan
[2]Department of Computer Science and Information Engineering, National Taipei University, New Taipei City 23741, Taiwan
[3]Department of Neurology, Chang Gung Memorial Hospital, Taoyuan 33333, Taiwan

Corresponding authors: Yo-Ping Huang (yphuang@ntut.edu.tw) and Hung-Chou Kuo (kuo0426@adm.cgmh.org.tw)

This work was supported in part by the Ministry of Science and Technology, Taiwan, under Grant MOST108-2811-E-027-501, Grant MOST108-2321-B-027-001, and Grant MOST108-2221-E-027-111-MY3, and in part by the Joint Project between the National Taipei University of Technology and the Chang Gung Memorial Hospital under Grant NTUT-CGMH-106-05.

ABSTRACT Parkinson's disease (PD) is one of the serious diseases in the neurodegenerative disease group, whose early stage pre-diagnosis is still very tedious. Radiologists and medical practitioners mostly depended on the analysis of PD patients' magnetic resonance images (MRIs) to identify this disease. Due to presence of grayscale features and uncertain inherited information in MRIs, their pattern recognition and visualization were very complex. With this motivation, a new method for analyzing and visualizing patterns in MRI images was presented in this study. For this purpose, this study adopted fuzzy information gain (FIG) function and K-means clustering algorithm. The FIG function was used to quantify the fuzzified pixels information, whereas K-means clustering algorithm was employed to cluster those fuzzified pixels information. Finally, changes in MRIs were recognized and classified into three distinct regions, viz., the minimum changed region (MINCR), the maximum changed region (MAXCR) and the average changed region (AVGCR). Experimental results were provided by comparing PD patients' segmented MRIs with seven well-known image segmentation methods, including adaptive threshold method, watershed method, gray threshold method, fuzzy based method, K-means clustering algorithm, adaptive K-means clustering algorithm and fuzzy c-means (FCM) algorithm. The proposed method achieved an average mean squared error of 63.49, peak signal-to-noise ratio of 30.14 and Jaccard similarity coefficient of 0.92 among nine MRIs of PD. The performance showed an improvement of 20.73%-32.94%, 3.54%-6.20% and 6.98%-64.29% over the average mean squared error, peak signal-to-noise ratio and Jaccard similarity coefficient, respectively compared to other image segmentation methods.

INDEX TERMS Fuzzy information gain, image segmentation, K-means clustering, magnetic resonance images (MRIs), Parkinson's disease (PD).

I. INTRODUCTION

To develop pattern recognition and vision method for medical images has become one of the most challenging tasks in view of practical as well as industrial interest [1]–[3]. The medical image segmentation method helps to discover uniform objects alongside their edges and textures [4]. However, MRI segmentation is a very tedious task due to their inherited uncertain structures and inhomogeneities in grayscale intensities [5]. For efficient and faster decision-making, radiologists and medical practitioners highly depended on MRIs [6]. For this reason, image analysts or computer vision experts engaged in developing many algorithms for MRIs segmentation, which differed from objective to objective [7]. By this motivation, an effort is made in this paper to develop segmentation method for the MRIs.

PD is one of the severe neurodegenerative diseases, the pre-diagnosis of which remains very cumbersome at an early stage, as it depends primarily on clinical or medical evidence. This disease involves motor symptom dysfunction such as

The associate editor coordinating the review of this manuscript and approving it for publication was Muhammad Imran Tariq.

tremor, trembling, slow motion (bradykinesia) and altered gait [8]. Despite serious attention given for developing standard tests or methods based on a blood sample or image analysis by the scientific community, there is still no efficient solution for early detection of PD. The experts use positron emission tomography (PET) or single-photon emission computerized tomography (SPECT) scans to evaluate the level of PD [9]. Those two scanning techniques are, however, too costly and are only used in specialized laboratories. Physicians diagnose this disease very lately in most cases, and make delayed decisions for the treatment of this disease when the neuron system of the patients nearly destroyed. In medical terms, the critical stage of this disease is known as Braak Stage III-IV [10].

For the pre-diagnosis of PD, use of CT (computed tomography) or MRI scan has been increased recently. However, diagnosis of PD using MRI suffers from the following issues such as:

1) In most of the cases, MRI of PD patients seem to be normal or no significant changes [11]. Hence, MRI scanning is useful only for recognizing secondary diseases caused by the PD.
2) Tredici *et al.* [12] addressed that first structural damages due to PD came into notice after 10 years. MRI scanning is not clearly able to differentiate PD patients and non-PD patients [13].
3) Imaging techniques can only be able to identify the structural changes in brainstem for PD [14]. They are only helpful to diagnose the premotor disease and its progression.
4) Notwithstanding development in digital imaging, experts still rely on the grayscale MRIs for preparing reports [15]. Due to this reason, it is quite likely that severely affected regions have not been recognized in the human's brain.

This study introduces a new segmentation method using the proposed FIG and K-means clustering algorithm. Main objectives are to resolve the problems associated with analyzing the MRIs. The research objectives and contributions of the study are discussed next.

1) *To identify a method for uncertainty representation in MRIs*: For this problem, this study found it suitable to use fuzzy set theory [16]. Based on this theory, this study used the concept of fuzzy information (FI) [17]. This FI provides a unique facility by combining uncertain information along with its degree of membership together. This FI forms the basis of representing uncertain changes in respective MRIs by integrating all FI together.
2) *To quantify the changes in MRIs:* This study used the FIG function to measure the changes in terms of information [17]. Based on the degree of memberships associated with each FI, this FIG function can quantify the amount of uncertainty available for particular changes in MRIs. Based on this FIG function, this study has also explored to identify the region of maximum, minimum and average changes in MRIs.
3) *To recognize the changes in MRIs:* After quantification of uncertainty using FIG function, we carried out to recognize the significant changes in MRIs. These changes were classified as the MAXCR, MINCR and AVGCR. For recognizing and locating those changes efficiently, this study used K-means clustering algorithm [18], where FIG values associated with corresponding MRIs were used as inputs in this algorithm.

TABLE 1. List of terms, abbreviations and notations.

Terms	Abbreviation	Notation
Parkinson's disease	PD	–
Magnetic resonance image	MRI	–
Fuzzy information	FI	$\tilde{F}$
Fuzzy information system	FIS	$\tilde{K}$
Fuzzy information gain	FIG	$E(\tilde{F})$
Gray pixel space	GPS	G_s
Fuzzified entropy matrix	FEM	$\tilde{F}_{EM}$
Minimum changed region	MINCR	–
Maximum changed region	MAXCR	–
Average changed region	AVGCR	–
Joint region information function	JRIF	–
Mean squared error	MSE	MSE
Peak signal-to-noise ratio	PSNR	PSNR
Jaccard similarity coefficient	JSC	$J_{I_{input},I_{output}}(g)$
Correlation coefficient	CC	r

PD MRIs were employed for the experimental purpose [19], whose descriptions are provided in the subsequent section. Empirical analysis revealed the effectiveness of the proposed method over the existing well-known image segmentation methods. List of terms, abbreviations and notations used throughout the article are presented in Table 1.

The rest of this article is arranged as follows. Section II presents related works in image segmentation. Section III introduces mathematical formulation for uncertainty representation in image. The proposed method for segmentation of MRIs is discussed in Section IV. The findings of experiments are illustrated in Section V. Finally, Section VI deals with the conclusion and future directions.

II. RELATED WORKS IN IMAGE SEGMENTATION

In image processing and pattern recognition, image segmentation is one of the tedious tasks, which have many applications in the domain of computer vision, robotics, object detection, features extraction, and so forth [20]. However, image segmentation is a troublesome mechanism due to involvement of complexities in terms of contrast, brightness, noise, etc [21]. The main purpose of image segmentation is to separate each important object from the rest of the objects [22]. Hence, it is a mechanism of partitioning an image into various parts in such a way that each part has its own area. According to Cheng *et al.* [23], it is a method of partitioning

an image I into non-overlapping areas A_I:

$$\bigcup_{i=1}^{n} A_I = I, \text{ and } A_{I1} \cap A_{I2} = \emptyset, I1 \neq I2 \tag{1}$$

Grayscale image segmentation methods are basically based on partitioning an image by detecting discontinuous gray level values in a particular region [24]. If there is a homogeneity in gray level values of a particular region, then such a partition is done using clustering, thresholding, edge detection, etc [23]. In image processing and pattern recognition, there are numerous benchmark methods available, which include global thresholding method [25], gray threshold method [25], adaptive threshold method [26] and watershed method [27].

In image processing and pattern recognition, fuzzy set theory is broadly used due to its capability to deal with uncertainty very precisely. Tobias and Seara [22] proposed an image segmentation approach by providing threshold to histogram based on the similarity between gray levels, which is assessed through fuzzy measure. Chaira and Ray [28] used four types of fuzzy thresholding approaches, where membership value of each pixel is defined using Gamma membership function. Various applications of fuzzy set theory in image segmentation can be found in these articles [28]–[31].

Atanassov [32] proposed an intuitionistic fuzzy set (IFS) theory, which is recently used in image processing. Rather than assigning only one degree of membership to a pixel as in the case of fuzzy set theory based approaches, IFS can assign the degrees of memberships based on hesitant information [33]. In IFS, degree of membership of hesitant information is determined using two functions, viz., degree of membership and degree of non-membership. Melo-Pinto *et al.* [34] presented a method based on IFS for determining whether the pixel belongs to the background or the object. Then, by using a multilevel threshold method, their proposed method performed the image segmentation. Ananthi *et al.* [35] introduced a new image segmentation method on the basis of constructing IFS from multiple fuzzy sets. Verma *et al.* [36] used intuitionistic fuzzy c-means (IFCM) algorithm, which is a modified version of FCM, in brain image segmentation. Ananthi *et al.* [37] presented a new IFS based clustering algorithm to analyze brain tumor using MRIs.

In image segmentation, clustering algorithms were widely used. Based on their applications, they can be categorized into hard clustering and soft clustering algorithms. Hard clustering algorithm helps in finding natural boundaries for the objects, whereas soft clustering algorithm performs the same operation by identifying the fuzzy boundaries for the objects [38]. One of the most common algorithms in the hard clustering group is the K-means clustering algorithm [18], which assigns each color pixel to the particular cluster based on some distance criteria [39], [40]. The soft clustering algorithm such as Fuzzy c-means (FCM) [41] is commonly used for representing the objects in non-overlapping manner. FCM carries out segmentation based on fuzzy classification, where each pixel may have different membership degrees in different classes [42], [43]. In pattern recognition domain, numerous applications of the FCM algorithm have been reported in the literature [44]–[47]. Cinque *et al.* [48] introduced a modified fuzzy approach for image segmentation by defining a simple model, which is able to instance a prototype for each cluster. Zhao *et al.* [49] proposed a new a multiobjective spatial fuzzy clustering algorithm for segmenting noisy images.

III. MATHEMATICAL FORMULATION FOR UNCERTAINTY REPRESENTATION

For a problem space, if every *event* is considered as an individual uncertain information, then it can be represented by its corresponding degree of membership using the fuzzy set. Assuming $U = \{e_1, e_2, \ldots, e_n\}$ represents a universe of discourse for n number of events, where $i = 1, 2, \ldots, n$. Various changes in these events can be characterized by categorizing them as *low change*, *moderate change*, *high change*, and so on. For the representation of such changes, we can use the fuzzy set theory. For the universe of discourse U, we can define the fuzzy set $\tilde{X}$ based on the events by

$$\tilde{X} = \mu(e_1)/e_1 + \mu(e_2)/e_2 + \ldots + \mu(e_n)/e_n \tag{2}$$

Here, μ represents the degree of membership function used in the fuzzy set theory. Hence, $\mu(e_i)$ gives the degree of membership value between range [0, 1] for the event e_i that associated with the fuzzy set $\tilde{X}$. Here, the symbol "+" denotes the fuzzy union operation and the symbol "/" denotes the separator rather than the commonly used summation and division in algebra, respectively.

Singh and Dhiman [17] introduced the concept of FI on the basis of the above Fuzzy set formulation. Here, we will correlate this concept for the better analysis of MRIs. A FI contains an uncertain set of events and their related fuzzified information. It can be defined for the universe of discourse U as follows.

Definition 1: (FI). A FI for the event e_i is a paired set of elements $\{e_i, \mu(e_i)\}$, $i = 1, 2, \ldots, n$, which can be denoted by $\tilde{F}$. Mathematically, it can be expressed as:

$$\tilde{F} = \{e_i, \mu(e_i)\}/U, \quad \forall e_i \in U \tag{3}$$

The FI does not often give full descriptions of the uncertainty for a given event. In problem space, complete information about the inherent uncertainty can be given by integrating these FI associated with the events. Such a collection of FI, therefore, constitutes a system called FIS. Mathematically, it can be expressed as follows.

Definition 2: (FIS). The FIS is a set of FI defined on the U. It is denoted by $\tilde{K}$. It can be expressed, mathematically, as:

$$\tilde{K} = [\{e_1, \mu(e_1)\}/U, \{e_2, \mu(e_2)\}/U, \ldots, \{e_n, \mu(e_n)\}/U] \tag{4}$$

Here, each $\{e_i, \mu(e_i)\}/U$ denotes the individual FI defined based on the U, where $e_i \in U$ and $\mu(e_i) \in [0, 1]$.

To quantify the fuzziness involved in each FI, FIG function [17] is used. The FIG function can be expressed as follows.

Definition 3: (FIG). It is a function to quantify uncertainty represented in terms of FI for the set of uncertain events defined in the universe of discourse U. Mathematically, it can be expressed as:

$$E(\tilde{F}) = -\sum_{i=1}^{n} \mu(e_i) \log_2(\mu(e_i)) \tag{5}$$

Here, $e_i \in U$, and $\mu(e_i) \in [0, 1]$. In Eq. (5), the $E(\tilde{F})$ is called the FIG function.

IV. THE PROPOSED METHOD

This section introduces the proposed method for the segmentation of MRIs based on FIG and K-means clustering algorithm. Each step of the proposed method is explained in the subsequent subsection.

A. REPRESENTATION OF PIXELS

For an image I_{input}, various changes can be distinguished in terms of color intensities that are associated with those pixels. By combining those pixels, a space can be defined for the I_{input}, which can be termed as a *gray pixel space (GPS)*. In the following, we will introduce a definition for the GPS in context of I_{input}.

*Definition 4: **(GPS)**. For an input image I_{input}, it has L levels with $X_{i,j}$ gray level at (i, j) pixel location. A GPS is a collection of $X_{i,j}$ gray pixels that form a space in the image. The GPS for the image I_{input} can be represented as G_s. Mathematically, it can be expressed in the following matrix form.*

$$G_s = \begin{bmatrix} X_{1,1} & X_{1,2} & \dots & X_{1,n} \\ X_{2,1} & X_{2,2} & \dots & X_{2,n} \\ \vdots & \vdots & \ddots & \vdots \\ X_{m,1} & X_{m,2} & \dots & X_{m,n} \end{bmatrix} \tag{6}$$

where, the maximum number of rows and columns for the I_{input} are denoted by the m and n, respectively. Here, $i = 1, 2, \dots, m$ and $j = 1, 2, \dots, n$.

B. FORMATION OF FIS

In the representation of the GPS, there is an absence of clear boundary of each special object, which is hard to be classified as a changed or unchanged pixel. The representation of such pixels that belong to the GPS is an uncertain concept. This inherent uncertainty of nature leads us towards the representation of pixels in terms of FIS. In the following, we formulate the FIS for each pixel that belongs to the GPS.

*Definition 5: **(FIS for the GPS)**. It is a collection of FI for each pixel that belongs to the GPS. Mathematically, it can be represented as:*

In Eq. (7), as shown as bottom of the next page, each $\{X_{i,j}, \mu(X_{i,j})\}/U$ represents individual FI of the crisp pixel $X_{i,j} \in U$ and $\mu(X_{i,j}) \in [0, 1]$.

```
1: procedure PERFORM_CLUSTERING()
2:     Input: image I_input with L levels and gray level
   pixel
3:     X_{i,j} at (i, j) pixel position, where i = 1, 2, ..., m
4:     and j = 1, 2, ..., n.
5:     for ∀X_{i,j}
6:         Represent I_input as the GPS.
7:         Convert GPS into the FIS.
8:         Prepare the FEM from the FIS.
9:         Apply the K-means clustering algorithm in the
10:        FEM.
11:    end for
12:    Output: segmented image I_output with K number of
13:    clustered FIG values.
14: procedure PERFORM_VISUALIZATION()
15:    Input: K number of clustered FIG values in the form
16:    E(μ(X_{i,j})), where i = 1, 2, ..., m and
17:    j = 1, 2, ..., n.
18:    for ∀E(μ(X_{i,j}))
19:        Classify the FEM into three regions, viz.,
20:        MINCR, MAXCR and AVGCR.
21:        Visualize different patterns using the JRIF,
22:        which includes paired set of regions,
23:        viz., J(MINCR, MAXCR),
24:        J(MINCR, AVGCR)
25:        and J(MAXCR, AVGCR).
26:    end for
27:    Output: classified image with three different re-
   gions.
```

FIGURE 1. Pseudo codes of the proposed method.

C. MEASURE OF UNCERTAINTY

The amount of information available in terms of degrees of memberships can be measured using the FIG function (Eq. 5). Using this function, the FIG value for the individual FI $\{X_{i,j}, \mu(X_{i,j})\}/U$ are obtained, and presented in a matrix form. We refer this matrix as the *fuzzified entropy matrix (FEM)*.

*Definition 6: **(FEM)**. It is a matrix, where each FI is represented in terms of its corresponding FIG value. The FEM is denoted as $\tilde{F}_{EM}$. It can be defined as:*

$$\tilde{F}_{EM} = \begin{bmatrix} E(\mu(X_{1,1})) & E(\mu(X_{1,2})) & \dots & E(\mu(X_{1,n})) \\ E(\mu(X_{2,1})) & E(\mu(X_{2,2})) & \dots & E(\mu(X_{2,n})) \\ \vdots & \vdots & \ddots & \vdots \\ E(\mu(X_{m,1})) & E(\mu(X_{m,2})) & \dots & E(\mu(X_{m,n})) \end{bmatrix} \tag{8}$$

Here, $E(\mu(X_{i,j}))$ satisfies Eq. (3) and $\mu(X_{i,j}) \in \tilde{K}$.

D. CLUSTERING OF FEM

In this study, a set of pixels is assumed as a system, which is called the GPS. Now, it is obvious that if entropy of a particular pixel is changed in the GPS, then its corresponding gray level values will surely be changed. These changes can be studied using similarity and dissimilarity analysis of FIG

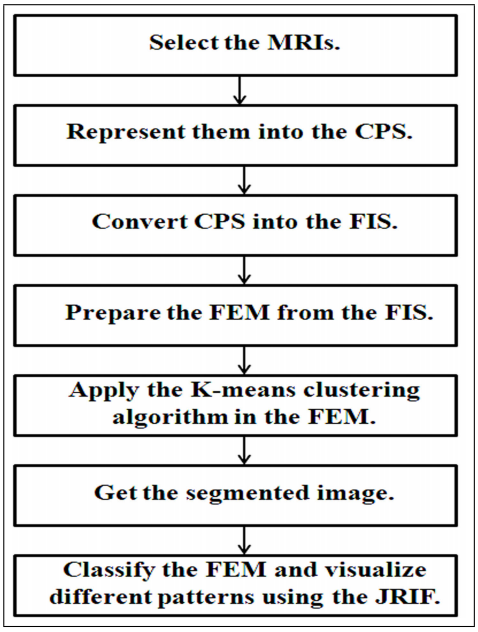

FIGURE 2. Flowchart of the proposed method.

values associated with the FEM. One of such techniques suitable for this kind of analysis is to employ clustering algorithms.

In the context of clustering FIG values available in the FEM, this study uses the K-means clustering algorithm. For each $E(\mu(X_{i,j})) \in \tilde{F}_{EM}$, the K-means clustering algorithm is able to generate k-number of clusters. Steps involved in this algorithm are explained next.

Step 1. Input:
$\tilde{F}_{EM}$: a FEM containing n number of FIG values in the form $E(\mu(X_{i,j}))$, where $i = 1, 2, \ldots, m$ and $j = 1, 2, \ldots, n$.
k: select the number of clusters.
Step 2. Select K initial clusters in space as:

$$Z_1(1), Z_2(1), \ldots, Z_k(1)$$

Here, 1 indicates the first iteration of the algorithm.
Step 3. repeat
Step 4. For the k^{th} iterative step, each $E(\mu(X_{i,j})) \in S_j(k)$ if the following relation is satisfied:

$$D(E(\mu(X_{i,j})), Z_j(k)) = \sum_{i=1}^{m}\sum_{j=1}^{n}\sqrt{(E(\mu(X_{i,j})) - Z_j(k))^2} \tag{9}$$

For $i = 1, 2, \ldots, K$, $i \neq j$, where $S_j(k)$ denotes the set of FIG values whose cluster centre is $Z_j(k)$.

Step 5. Compute the new cluster centres $Z_j(k+1)$ using the following equation as:

$$Z_j(k+1) = \frac{1}{N_j}\sum E(\mu(X_{i,j})), \quad \forall E(\mu(X_{i,j})) \in C_j(k) \tag{10}$$

where N_j is the number of FIG values in the $S_j(k)$ and $j = 1, 2, \ldots, K$.
Step 6. Goto **Step 3** until cluster centers do not modify any more.

Output: A set consists of K number of clustered FIG values.

E. PATTERN VISUALIZATION

In this study, the segmented MRIs are classified into three different regions, viz., MINCR, MAXCR and AVGCR. They can be defined as follows.

Definition 7: (MINCR, MAXCR and AVGCR). The MINCR, MAXCR and AVGCR can be defined based on the $\tilde{F}_{EM}$ as:

$$MINCR = \bigwedge_{i=1}^{m}\bigwedge_{j=1}^{n} E(\mu(X_{i,j})) \in \tilde{F}_{EM} \tag{11}$$

$$MAXCR = \bigvee_{i=1}^{m}\bigvee_{j=1}^{n} E(\mu(X_{i,j})) \in \tilde{F}_{EM} \tag{12}$$

$$AVGCR = \frac{MINCR + MAXCR}{2} \tag{13}$$

Here, the symbols $\bigwedge$ and $\bigvee$ represent the fuzzy intersection and union operations among the information associated with two regions.

In this study, more visualization impact will be given by considering the information available in the MINCR, MAXCR and AVGCR. For this purpose, information associated with any set of distinct regions $R = \{MINCR, MAXCR, AVGCR\}$ can be jointed together. This joint operation is performed by using the proposed function called as a *joint region information function (JRIF)*. In the following, this JRIF can be defined for the set of regions R as follows.

Definition 8: (JRIF). It is a collection of FIG values associated with the paired set of regions as $J(MINCR, MAXCR)$, $J(MINCR, AVGCR)$ and $J(MAXCR, AVGCR)$ from the R, where J represents the JRIF. Mathematically, it can be defined as:

$$J(MINCR, MAXCR) = \bigvee_{i=1}^{m}\bigvee_{j=1}^{n}\{MINCR, MAXCR\} \tag{14}$$

$$\tilde{K} = \begin{bmatrix} \{X_{1,1}, \mu(X_{1,1})\}/U & \{X_{1,2}, \mu(X_{1,2})\}/U & \ldots & \{X_{1,n}, \mu(X_{1,n})\}/U \\ \{X_{2,1}, \mu(X_{2,1})\}/U & \{X_{2,2}, \mu(X_{2,2})\}/U & \ldots & \{X_{2,n}, \mu(X_{2,n})\}/U \\ \vdots & \vdots & \ddots & \vdots \\ \{X_{m,1}, \mu(X_{m,1})\}/U & \{X_{m,2}, \mu(X_{m,2})\}/U & \ldots & \{X_{m,n}, \mu(X_{m,n})\}/U \end{bmatrix} \tag{7}$$

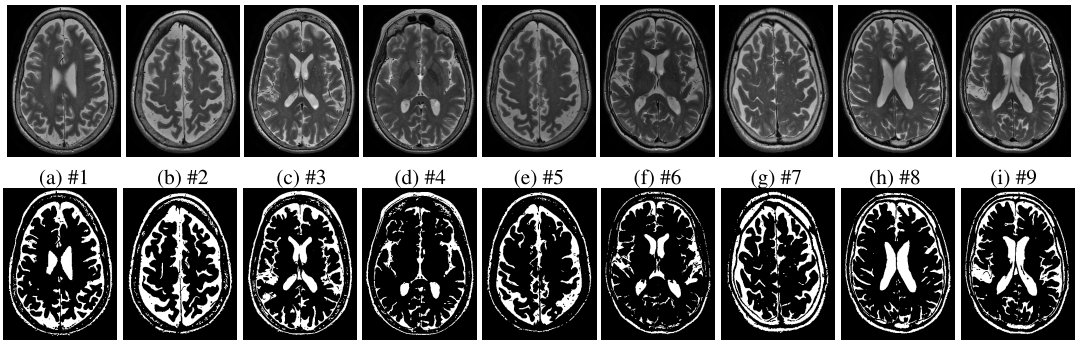

FIGURE 3. MRIs of PD patients with their respective GT images.

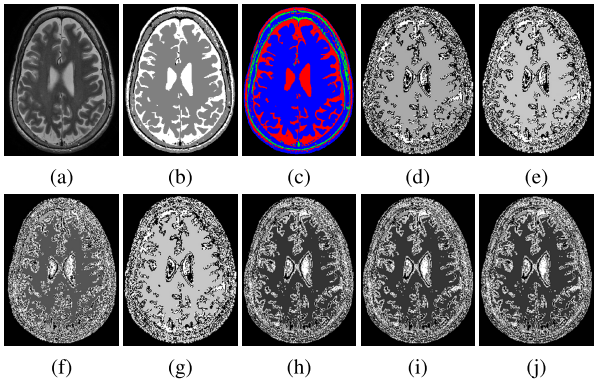

FIGURE 4. Segmentation of gray and white matters for image #1: (a) original image, (b) proposed method, (c) RGB effect of (b), (d) adaptive threshold method [26], (e) watershed method [50], (f) gray threshold method [25], (g) fuzzy based method [29], (h) K-means clustering algorithm [40], (i) adaptive K-means clustering algorithm [51], and (j) FCM algorithm [47].

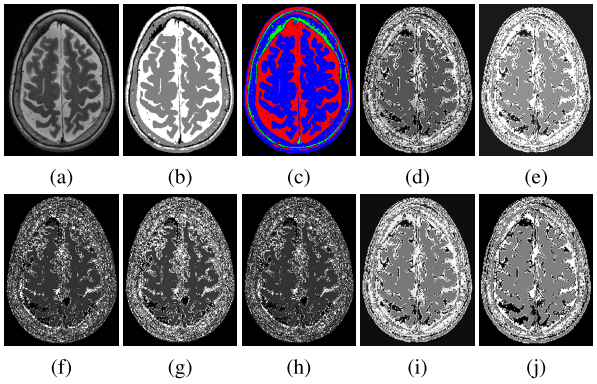

FIGURE 5. Segmentation of gray and white matters for image #2: (a) original image, (b) proposed method, (c) RGB effect of (b), (d) adaptive threshold method [26], (e) watershed method [50], (f) gray threshold method [25], (g) fuzzy based method [29], (h) K-means clustering algorithm [40], (i) adaptive K-means clustering algorithm [51], and (j) FCM algorithm [47].

$$J(MINCR, AVGCR) = \bigvee_{i=1}^{m} \bigvee_{j=1}^{n} \{MINCR, AVGCR\} \quad (15)$$

$$J(MAXCR, AVGCR) = \bigvee_{i=1}^{m} \bigvee_{j=1}^{n} \{MAXCR, AVGCR\} \quad (16)$$

Here, the symbol $\bigvee$ represents the fuzzy union operation among the information associated with two different regions.

The pseudo codes of the proposed method are presented in Fig. 1, which include two different procedures as PERFORM_CLUSTERING() and PERFORM_VISUALIZATION(). The procedure PERFORM_CLUSTERING() is used for segmenting the MRIs, while the procedure PERFORM_VISUALIZATION() is used for the pattern classification and visualization from the segmented MRIs. Fig. 2 shows a flowchart of the proposed method, which clearly describes its working process.

V. EXPERIMENTAL RESULTS

In this section, experimental results related to segmentation of MRIs of PD are discussed. To evaluate the performance of the proposed method, this study carried out experiments on MRIs images of PD. This dataset was acquired from the Image and Data Archive (IDA) [19]. Selected MRIs are shown in Fig. 3(a)-(i) along with their respective ground truth (GT) images.

A. EXPERIMENTAL SET-UP

The proposed method was developed based on Matlab version R2019a, which was running on a system with Microsoft Windows 10 Home, 64 bits operating system, Core i7-9700F processor, 16 GB main memory and 3.00 GHz CPU. In the course of the experiment, the universe of discourse for the I_{input} was assumed as $U = [\min(I_{input}), \max(I_{input})]$, where min and max give the minimum and maximum grayscale values from the I_{input}, respectively. Then, the FEM (Eq. 8) was defined to start the segmentation process on the basis of K-means clustering algorithm.

B. PERFORMANCE EVALUATION METRICS

The performance of the proposed method was evaluated using the well-known parameters used in image segmentation analysis. These selected metrics include mean squared error

TABLE 2. Comparison of MSE Obtained by the Proposed Method and Existing Methods for the MRIs of PD.

Method	#1	#2	#3	#4	#5	#6	#7	#8	#9	Average
Adaptive [26]	95.11	93.11	93.16	94.54	96.91	94.11	95.34	93.45	96.34	94.67
Watershed [50]	96.11	95.24	93.12	94.23	94.26	95.23	92.33	96.23	93.16	94.43
Gray [25]	93.11	92.23	93.14	93.16	93.19	92.21	92.33	94.36	94.26	93.11
Fuzzy [29]	84.23	85.23	83.14	85.11	89.23	84.55	84.66	87.55	88.44	85.79
K-means [40]	83.14	82.23	83.14	81.30	83.55	84.56	81.44	83.56	85.56	83.16
Adaptive K [51]	81.14	81.23	82.14	81.30	82.55	81.56	81.44	81.56	83.56	81.83
FCM [47]	79.23	79.24	78.34	81.13	80.65	80.45	79.34	80.78	81.66	80.09
Proposed	**65.17**	**60.71**	**64.92**	**62.33**	**65.46**	**63.23**	**62.67**	**63.78**	**63.17**	**63.49**

TABLE 3. Comparison of PSNR Obtained by the Proposed Method and Existing Methods for the MRIs of PD.

Method	#1	#2	#3	#4	#5	#6	#7	#8	#9	Average
Adaptive [26]	28.38	28.48	28.47	28.40	28.27	28.39	28.34	28.43	28.29	28.38
Watershed [50]	28.34	28.38	28.47	28.42	28.39	28.34	28.48	28.30	28.44	28.40
Gray [25]	28.47	28.52	28.47	28.47	28.44	28.48	28.48	28.38	28.39	28.46
Fuzzy [29]	28.91	28.86	28.97	28.86	28.63	28.86	28.85	28.71	28.66	28.81
K-means [40]	28.97	29.01	28.97	29.06	28.91	28.86	29.02	28.91	28.81	28.95
Adaptive K [51]	29.07	29.07	29.02	29.06	29.00	29.05	29.06	29.05	28.94	29.04
FCM [47]	29.18	29.18	29.23	29.07	29.06	29.08	29.14	29.06	29.01	29.11
Proposed	**30.02**	**30.33**	**30.04**	**30.22**	**30.01**	**30.16**	**30.19**	**30.12**	**30.16**	**30.14**

TABLE 4. Comparison of JSC Obtained by the Proposed Method and Existing Methods for the MRIs of PD.

Method	#1	#2	#3	#4	#5	#6	#7	#8	#9	Average
Adaptive [26]	0.55	0.54	0.57	0.58	0.57	0.57	0.59	0.54	0.53	0.56
Watershed [50]	0.65	0.54	0.57	0.65	0.64	0.71	0.64	0.69	0.73	0.65
Gray [25]	0.69	0.68	0.66	0.67	0.68	0.65	0.68	0.68	0.69	0.68
Fuzzy [29]	0.72	0.74	0.77	0.78	0.72	0.76	0.79	0.78	0.78	0.76
K-means [40]	0.79	0.77	0.79	0.77	0.79	0.79	0.79	0.79	0.78	0.78
Adaptive K [51]	0.80	0.83	0.81	0.82	0.81	0.81	0.82	0.81	0.80	0.81
FCM [47]	0.84	0.86	0.86	0.87	0.86	0.87	0.86	0.88	0.87	0.86
Proposed	**0.94**	**0.95**	**0.95**	**0.89**	**0.91**	**0.90**	**0.93**	**0.91**	**0.90**	0.92

(MSE), peak signal-to-noise ratio (PSNR), Jaccard similarity coefficient (JSC) and correlation coefficient (CC). These metrics are described on the basis of original image (I_{input}), segmented image (I_{output}) and GT image (I_{ground}) as follows.

- MSE [52]: The MSE is utilized to calculate an average gray level intensity value lost during the segmentation of the original image *Ip*. The lower MSE value indicates minimal intensity loss and generates a better segmented image I_{output}. Mathematically, it can be represented as:

$$MSE = \frac{1}{M \times N} \sum_{m=1}^{M} \sum_{n=1}^{N} (I_{input} - I_{output})^2 \quad (17)$$

  Here, $M \times N$ denotes the size of image in terms of pixels.
- PSNR [52]: The PSNR has a negative correlation with the MSE, so its higher value shows less distortion and generates a better segmented image I_{output}. Mathematically, it can be represented as:

$$PSNR = 10 \times \log_{10} \left[\frac{(255)^2}{MSE} \right] \quad (18)$$

- JSC [53]: The JSC measures the resemblance between two images. It can be described as the intersection of the pixel sets, divided by the size of the union of the pixel sets. The JSC value lies between the range [0, 1]. A similarity value close to 1 indicates that the segmented regions have a perfect similarity with GT image. It can be defined as:

$$J_{I_{output}, I_{ground}}(c) = \frac{X_{I_{output} \cap I_{ground}}(c)}{X_{I_{output} \cup I_{ground}}(c)} \quad (19)$$

  In Eq. 19, $X_{I_{output} \cap I_{ground}}(c)$ and $X_{I_{output} \cup I_{ground}}(c)$ represent the intersection and union of pixels that belong to the class c in case of both the segmented image and GT image, respectively.
- CC [54]: The CC measure is used to identify the match between the original image and the segmented image. The CC values lies between the range $[-1, 1]$. A CC value close to 1 indicates that the segmented regions have a perfect match with original image. It can be defined as:

$$r = \frac{\sum_{m=1}^{M} \sum_{n=1}^{N} (I_{input} - \bar{I}_p)(I_{output} - \bar{I}_{output})}{\left(\sum_{m=1}^{M} \sum_{n=1}^{N} (I_{input} - \bar{I}_{input})^2 \right) \left(\sum_{m=1}^{M} \sum_{n=1}^{N} (I_{output} - \bar{I}_{output})^2 \right)} \quad (20)$$

  where r denotes the CC value. In Eq. 20, $\bar{I}_{input}$ and $\bar{I}_{output}$ represent the means of original image and the segmented image, respectively.

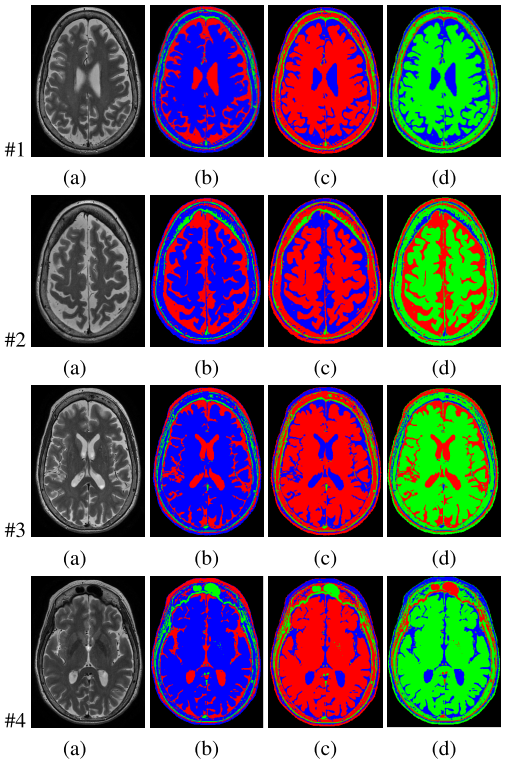

FIGURE 6. Classification of MRIs into three different regions for images #1–#4: (a) original image, (b) MINCR of (a), (c) MAXCR of (a), and (d) AVGCR of (a).

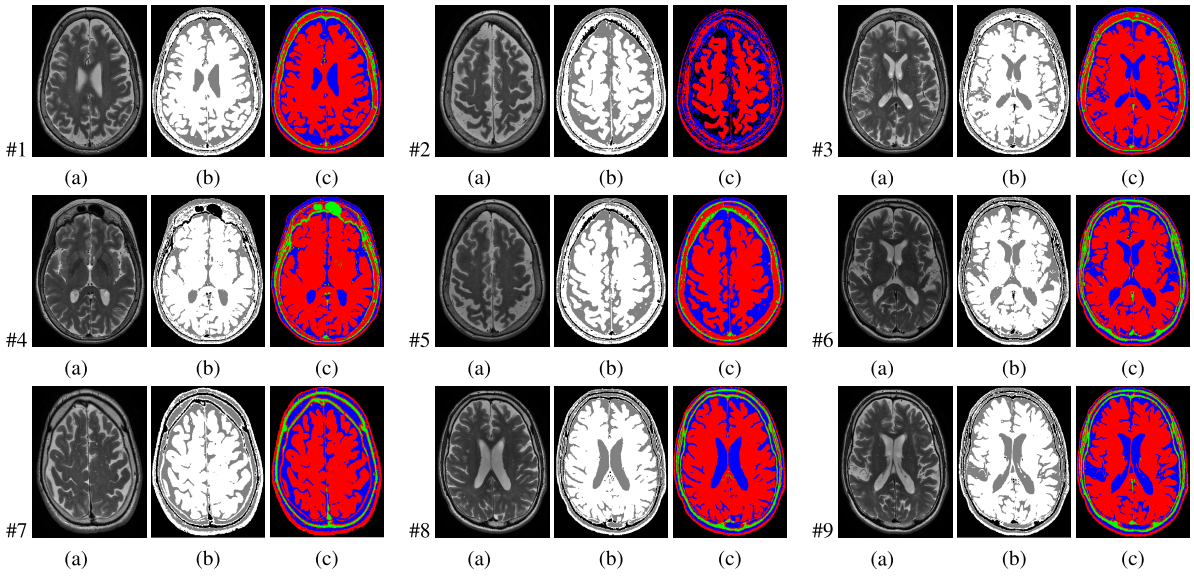

FIGURE 7. Patterns visualization of MRIs for images #1–#9: (a) original image, (b) J(MINCR, MAXCR) of (a), and (c) RGB effect of (b).

C. DISCUSSION ON SEGMENTATION OF MRI

Original MRIs and their corresponding segmented images are shown in Figs. 4-5 that are obtained from the proposed and existing methods, which include adaptive threshold method [26], watershed method [50], gray threshold method [25], fuzzy based method [29], K-means clustering algorithm [40], adaptive K-means clustering algorithm [51] and FCM algorithm [47]. Based on these segmented images, it can be easily observed that the different regions of the human brain were not uniformly segmented using the existing methods. Comparing segmented images with segmented images obtained from the proposed method, it is clear that the regions of the brain are adequately segmented. Segmented images based on the existing methods shown in Figs 4-5 revealed that previous methods can not manage such images because of inconsistent and ambiguous boundaries. On the other hand, the results obtained using the proposed method clearly segmented such images, where boundaries and objects can be easily separated (in Figs. 4-5(b)).

For the better visualization of segmented information, each segmented image was presented through the RGB effect. For images #1–#2, their corresponding RGB effect images were shown in Fig. 4(c) and Fig. 5(c), respectively.

Finally, statistical analyzes of the proposed method and existing methods were conducted using the MSE, PSNR and JSC metrics. The efficiency of the proposed method was evaluated based on well-known methods that included adaptive threshold method [26], the watershed method [50], the gray threshold method [25], the fuzzy method [29], the K-means clustering algorithm [40], the adaptive K-means clustering algorithm [51], and the FCM algorithm [47]. Table 2 presents the comparisons of the proposed method with other methods in terms of the average MSE values. For images #1–#9, adaptive threshold method [26], watershed method [50], gray threshold method [25], fuzzy based method [29], K-means clustering algorithm [40], adaptive K-means clustering algorithm [51] and FCM algorithm [47] had average MSE values of 94.67, 94.43, 93.11, 85.79, 83.16, 81.83 and 80.09, respectively. By contrast, the proposed method achieved an average MSE value of 63.49, which showed significant improvement ranging 20.73%-32.94% over other methods. For the comparisons of average PSNR they were shown in 3. The average PSNR values from the adaptive threshold method [26], watershed method [50], gray threshold method [25], fuzzy based method [29], K-means clustering algorithm [40], adaptive K-means clustering algorithm [51] and FCM algorithm [47] were 28.38, 28.40, 28.46, 28.81, 28.95, 29.04 and 29.11, respectively. By contrast, the proposed method exhibited average PSNR value of 30.14, which showed improvement in average PSNR values over other methods by 3.54%-6.20%. Table 4 shows comparisons of the average JSC for the proposed method with other methods. The average JSC values obtained from other seven methods were 0.56, 0.65, 0.68, 0.76, 0.78, 0.81 and 0.86, respectively. The proposed method achieved an average JSC value of 0.92, which again showed significant improvement of 6.98%-64.29% compared to other methods. These statistical analyses revealed that the proposed method outperformed existing methods for MRIs segmentation of PD.

D. DISCUSSION ON PATTERN CLASSIFICATION AND VISUALIZATION

We have performed the CC analysis among the original MRIs and the three different regions categorized as the MINCR, MAXCR and AVGCR. These three different classified regions for the original images #1–#4 are shown in Fig. 6(b)-(d), respectively. The CC exhibited by the original MRIs and three different regions are presented in Table 5. The CC values indicated matching of regions among the original MRIs and three different regions. In Table 5, the CC values corresponding to the MINCR indicated minimum matching (Fig. 6(b)) quantified through the MRIs (Fig. 6(b)). The

TABLE 5. The Correlation Coefficient Analysis of Three Different Regions of MRIs.

Image	MINCR	MAXCR	AVGCR
#1	0.72	0.84	0.78
#2	0.76	0.83	0.79
#3	0.86	0.89	0.86
#4	0.74	0.90	0.82
#5	0.84	0.89	0.86
#6	0.74	0.91	0.82
#7	0.76	0.80	0.77
#8	0.75	0.83	0.79
#9	0.83	0.83	0.83

radiologists and medical practitioners can use the images related to the MINCR for identifying and locating minor changes in human brain during PD. Similarly, the CC values corresponding to the MAXCR indicated maximum matching as depicted in Table 5. The MAXCR related images (Fig. 6(c)) can be used for identifying and locating maximum changes in human brain during PD. The CC values corresponding to the AVGCR indicated average matching as depicted in Table 5. These images (Fig. 6(d)) can be used for identifying and locating moderate changes in human brain during PD.

For generating more significant patterns through the segmentation, further experiment was carried out to visualize them by combining the FIG values associated with the MINCR and MAXCR. For this purpose, J(MINCR, MAXCR) function was utilized. These results are shown in Fig. 7(b) for the images #1–#9, where patterns of human brain during PD were clearly visualized. The RGB effect was also provided to create more visual impact for the patterns as shown in Fig. 7(c). Based on the results, it was obvious that the J(MINCR, MAXCR) function highlighted the inherited information from the MINCR and MAXCR together. The proposed method was also able to recognize the patterns as well as able to provide good visual information.

MRI classification with three different regions, i.e. MINCR, MAXCR and AVGCR, were shown in Fig. 6. MRI classification regions defined by the J(MINCR, MAXCR) function were shown in Fig. 7. These classification regions were obtained through the segmented MRIs. In these figures, RGB effect was provided to the MRIs classification regions to represent different inherent patterns. The RGB effect is device-dependent in nature [54], [55], so the different color combinations were observed in the MRI classification regions described by the MINCR, MAXCR, AVGCR and J(MINCR, MAXCR).

VI. CONCLUSION AND FUTURE DIRECTIONS

For computer-vision researchers, successful segmentation of the MRI remains an issue. This study was conducted to investigate MRIs of PD patients using the proposed segmentation approach based on hybridization of FIS, FIG and K-means clustering algorithm. FIS was used to prepare a fuzzified information system for the grayscale pixels and helped to represent them in terms of degrees of memberships. Then, inherited uncertainty associated with each pixel was obtained using the FIG function. Based on these FIG values, the FEM was prepared. The K-means clustering algorithm was applied on the FEM to group FIG values based on their similarity and dissimilarity. The K-means clustering algorithm determines the similarity and dissimilarity among the FIG values based on the well-defined distance function. In this study, region available in MRIs was classified into three different categories as the MINCR, MAXCR and AVGCR. Results showed that each distinct category of region carried different information, which can help radiologists and medical practitioners for the pre-diagnosis of PD in early stage. For analyzing and visualizing the patterns more effectively, the JRIF function was utilized. This function was able to reflect significant patterns in the segmented MRIs by considering information of the MINCR and MAXCR. The segmented MRIs based on the JRIF can help the medical experts to analyze the changes in MRIs very precisely. The proposed approach was evaluated with the MSE, PSNR, JSC and CC metrics. Empirical analysis demonstrated the effectiveness of the proposed method over the well-known image segmentation methods.

The study's limitation was that the suggested approach was only validated with MRIs of PD patients. The proposed approach may be improved in the future in such a way that it can be applied to other types of MRIs.

REFERENCES

[1] G. Wang, "A perspective on deep imaging," *IEEE Access*, vol. 4, pp. 8914–8924, 2016.

[2] Y. Liu, K. Sung, G. Yang, S. A. Mirak, M. Hosseiny, A. Azadikhah, X. Zhong, R. E. Reiter, Y. Lee, and S. S. Raman, "Automatic prostate zonal segmentation using fully convolutional network with feature pyramid attention," *IEEE Access*, vol. 7, pp. 163626–163632, 2019.

[3] K. Xu, J. Cao, K. Xia, H. Yang, J. Zhu, C. Wu, Y. Jiang, and P. Qian, "Multichannel residual conditional GAN-leveraged abdominal pseudo-CT generation via Dixon MR images," *IEEE Access*, vol. 7, pp. 163823–163830, 2019.

[4] *IEEE Recommended Practice for Three-Dimensional (3D) Medical Modeling*, Standard 3333.2.1-2015, IEEE Computer Society, New York, USA, Feb. 2015.

[5] D. Pham and J. Prince, "Adaptive fuzzy segmentation of magnetic resonance images," *IEEE Trans. Med. Imag.*, vol. 18, no. 9, pp. 737–752, Sep. 1999.

[6] Z. Tu and X. Bai, "Auto-context and its application to high-level vision tasks and 3D brain image segmentation," *IEEE Trans. Pattern Anal. Mach. Intell.*, vol. 32, no. 10, pp. 1744–1757, Oct. 2010.

[7] Y.-P. Huang, S. M. M. Zaza, W.-J. Chu, R. Krikorian, and F. E. Sandnes, "Using fuzzy systems to infer memory impairment from MRI," *Int. J. Fuzzy Syst.*, vol. 20, no. 3, pp. 913–927, Mar. 2018.

[8] J. A. Stamford, P. N. Schmidt, and K. E. Friedl, "What engineering technology could do for quality of life in Parkinson's disease: A review of current needs and opportunities," *IEEE J. Biomed. Health Inform.*, vol. 19, no. 6, pp. 1862–1872, Nov. 2015.

[9] M. Agrawal and A. Biswas, "Molecular diagnostics of neurodegenerative disorders," *Frontiers Mol. Biosci.*, vol. 2, pp. 1–10, Sep. 2015.

[10] H. Braak, K. D. Tredici, U. Rüb, R. A. D. Vos, E. N. J. Steur, and E. Braak, "Staging of brain pathology related to sporadic Parkinson's disease," *Neurobiol. Aging*, vol. 24, no. 2, pp. 197–211, Mar. 2003.

[11] L. Badea, M. Onu, T. Wu, A. Roceanu, and O. Bajenaru, "Exploring the reproducibility of functional connectivity alterations in Parkinson's disease," *PLoS ONE*, vol. 12, no. 11, Nov. 2017, Art. no. e0188196.

[12] K. D. Tredici, U. Rüb, R. A. De Vos, J. R. Bohl, and H. Braak, "Where does Parkinson disease pathology begin in the brain?" *J. Neuropathol. Exp. Neurol.*, vol. 61, no. 5, pp. 413–426, May 2002.

[13] A. Nagano-Saito, Y. Washimi, Y. Arahata, T. Kachi, J. P. Lerch, A. C. Evans, A. Dagher, and K. Ito, "Cerebral atrophy and its relation to cognitive impairment in Parkinson disease," *Neurology*, vol. 64, no. 2, pp. 224–229, Jan. 2005.

[14] A. J. Stoessl, W. W. Martin, M. J. McKeown, and V. Sossi, "Advances in imaging in Parkinson's disease," *Lancet Neurol.*, vol. 10, no. 11, pp. 987–1001, Nov. 2011.
[15] A. Ogura, A. Kamakura, Y. Kaneko, T. Kitaoka, N. Hayashi, and A. Taniguchi, "Comparison of grayscale and color-scale renderings of digital medical images for diagnostic interpretation," *Radiol. Phys. Technol.*, vol. 10, no. 3, pp. 359–363, Sep. 2017.
[16] C. V. Negoita, "Fuzzy sets," *Fuzzy Sets Syst.*, vol. 133, no. 2, p. 275, Jan. 2003.
[17] P. Singh and G. Dhiman, "Uncertainty representation using fuzzy-entropy approach: Special application in remotely sensed high-resolution satellite images (RSHRSIs)," *Appl. Soft Comput.*, vol. 72, pp. 121–139, Nov. 2018.
[18] J. M. Queen, "Some methods for classification and analysis of multivariate observations," in *Proc. 5th Berkeley Symp. Math. Statist. Probab.*, Oakland, CA, USA, 1967, vol. 1, no. 14, pp. 281–297.
[19] University of Southern California, Los Angeles, CA, USA. (2019). *Image and Data Archive*. [Online]. Available: https://ida.loni.usc.edu/
[20] Y. Li, Y. Guo, Y. Kao, and R. He, "Image piece learning for weakly supervised semantic segmentation," *IEEE Trans. Syst., Man, Cybern., Syst.*, vol. 47, no. 4, pp. 648–659, Apr. 2017.
[21] X. Yang, W. Zhao, Y. Chen, and X. Fang, "Image segmentation with a fuzzy clustering algorithm based on ant-tree," *Signal Process.*, vol. 88, no. 10, pp. 2453–2462, Oct. 2008.
[22] O. Tobias and R. Seara, "Image segmentation by histogram thresholding using fuzzy sets," *IEEE Trans. Image Process.*, vol. 11, no. 12, pp. 1457–1465, Dec. 2002.
[23] H. Cheng, X. Jiang, Y. Sun, and J. Wang, "Color image segmentation: Advances and prospects," *Pattern Recognit.*, vol. 34, no. 12, pp. 2259–2281, Dec. 2001.
[24] P. Hurtik, N. Madrid, and M. Dyba, "Sensitivity analysis for image represented by fuzzy function," *Soft Comput.*, vol. 23, no. 6, pp. 1795–1807, Mar. 2019.
[25] N. Otsu, "A threshold selection method from gray-level histograms," *IEEE Trans. Syst., Man, Cybern.*, vol. SMC-9, no. 1, pp. 62–66, Jan. 1979.
[26] D. Bradley and G. Roth, "Adaptive thresholding using the integral image," *J. Graph. Tools*, vol. 12, no. 2, pp. 13–21, Jan. 2007.
[27] L. Vincent and P. Soille, "Watersheds in digital spaces: An efficient algorithm based on immersion simulations," *IEEE Trans. Pattern Anal. Mach. Intell.*, vol. 13, no. 6, pp. 583–598, Jun. 1991.
[28] T. Chaira and A. Ray, "Threshold selection using fuzzy set theory," *Pattern Recognit. Lett.*, vol. 25, no. 8, pp. 865–874, Jun. 2004.
[29] T. Chaira and A. Ray, "Segmentation using fuzzy divergence," *Pattern Recognit. Lett.*, vol. 24, no. 12, pp. 1837–1844, Aug. 2003.
[30] K. C. Ciesielski and J. K. Udupa, "Affinity functions in fuzzy connectedness based image segmentation I: Equivalence of affinities," *Comput. Vis. Image Understand.*, vol. 114, no. 1, pp. 146–154, Jan. 2010.
[31] J. Lan and Y. Zeng, "Multi-threshold image segmentation using maximum fuzzy entropy based on a new 2D histogram," *Optik-Int. J. Light Electron Opt.*, vol. 124, no. 18, pp. 3756–3760, Sep. 2013.
[32] K. T. Atanassov, "Intuitionistic fuzzy sets," *Fuzzy Sets Syst.*, vol. 20, no. 1, pp. 87–96, Aug. 1986.
[33] P. Balasubramaniam and V. Ananthi, "Image fusion using intuitionistic fuzzy sets," *Inf. Fusion*, vol. 20, pp. 21–30, Nov. 2014.
[34] P. Melo-Pinto, P. Couto, H. Bustince, E. Barrenechea, M. Pagola, and J. Fernandez, "Image segmentation using Atanassov's intuitionistic fuzzy sets," *Expert Syst. Appl.*, vol. 40, no. 1, pp. 15–26, 2013.
[35] V. Ananthi, P. Balasubramaniam, and C. Lim, "Segmentation of gray scale image based on intuitionistic fuzzy sets constructed from several membership functions," *Pattern Recognit.*, vol. 47, no. 12, pp. 3870–3880, Dec. 2014.
[36] H. Verma, R. Agrawal, and A. Sharan, "An improved intuitionistic fuzzy c-means clustering algorithm incorporating local information for brain image segmentation," *Appl. Soft Comput.*, vol. 46, pp. 543–557, Sep. 2016.
[37] V. P. Ananthi, P. Balasubramaniam, and T. Kalaiselvi, "A new fuzzy clustering algorithm for the segmentation of brain tumor," *Soft Comput.*, vol. 20, no. 12, pp. 4859–4879, Dec. 2016.
[38] H. Fritz, L. A. García-Escudero, and A. Mayo-Iscar, "Robust constrained fuzzy clustering," *Inf. Sci.*, vol. 245, pp. 38–52, Oct. 2013.
[39] Y. W. Lim and S. U. Lee, "On the color image segmentation algorithm based on the thresholding and the fuzzy C-means techniques," *Pattern Recognit.*, vol. 23, no. 9, pp. 935–952, Jan. 1990.
[40] H. Yao, Q. Duan, D. Li, and J. Wang, "An improved K-means clustering algorithm for fish image segmentation," *Math. Comput. Model.*, vol. 58, nos. 3–4, pp. 790–798, Aug. 2013.
[41] J. C. Bezdek, R. Ehrlich, and W. Full, "FCM: The fuzzy C-means clustering algorithm," *Comput. Geosci.*, vol. 10, nos. 2–3, pp. 191–203, Jan. 1984.
[42] S. Chen and D. Zhang, "Robust image segmentation using FCM with spatial constraints based on new kernel-induced distance measure," *IEEE Trans. Syst. Man, Cybern. B, Cybern.*, vol. 34, no. 4, pp. 1907–1916, Aug. 2004.
[43] Y. Guo, H. D. Cheng, and Y. Zhang, "A new neutrosophic approach to image denoising," *New Math. Natural Comput.*, vol. 5, no. 3, pp. 653–662, Nov. 2009.
[44] L. Ma and R. Staunton, "A modified fuzzy C-means image segmentation algorithm for use with uneven illumination patterns," *Pattern Recognit.*, vol. 40, no. 11, pp. 3005–3011, Nov. 2007.
[45] S. Balla-Arabe, X. Gao, and B. Wang, "A fast and robust level set method for image segmentation using fuzzy clustering and lattice Boltzmann method," *IEEE Trans. Cybern.*, vol. 43, no. 3, pp. 910–920, Jun. 2013.
[46] M. Gong, Y. Liang, J. Shi, W. Ma, and J. Ma, "Fuzzy C-means clustering with local information and kernel metric for image segmentation," *IEEE Trans. Image Process.*, vol. 22, no. 2, pp. 573–584, Feb. 2013.
[47] X.-L. Jiang, Q. Wang, B. He, S.-J. Chen, and B.-L. Li, "Robust level set image segmentation algorithm using local correntropy-based fuzzy C-means clustering with spatial constraints," *Neurocomputing*, vol. 207, pp. 22–35, Sep. 2016.
[48] L. Cinque, G. Foresti, and L. Lombardi, "A clustering fuzzy approach for image segmentation," *Pattern Recognit.*, vol. 37, no. 9, pp. 1797–1807, Sep. 2004.
[49] F. Zhao, H. Liu, and J. Fan, "A multiobjective spatial fuzzy clustering algorithm for image segmentation," *Appl. Soft Comput.*, vol. 30, pp. 48–57, May 2015.
[50] M. Zhang, L. Zhang, and H. Cheng, "A neutrosophic approach to image segmentation based on watershed method," *Signal Process.*, vol. 90, no. 5, pp. 1510–1517, May 2010.
[51] H. M. Moftah, A. T. Azar, E. T. Al-Shammari, N. I. Ghali, A. E. Hassanien, and M. Shoman, "Adaptive k-means clustering algorithm for MR breast image segmentation," *Neural Comput. Appl.*, vol. 24, nos. 7–8, pp. 1917–1928, Jun. 2014.
[52] Z. Wang, A. Bovik, H. Sheikh, and E. Simoncelli, "Image quality assessment: From error visibility to structural similarity," *IEEE Trans. Image Process.*, vol. 13, no. 4, pp. 600–612, Apr. 2004.
[53] O. Dalmau and M. Rivera, "A general Bayesian Markov random field model for probabilistic image segmentation," in *Combinatorial Image Analysis* (Lecture Notes in Computer Science), vol. 5852, P. Wiederhold and R. P. Barneva, Eds. Berlin, Germany: Springer, pp. 149–161, Nov. 2009.
[54] R. C. Gonzalez, R. E. Woods, and S. L. Eddins, *Digital Image Processing Using MATLAB*. Upper Saddle River, NJ, USA: Prentice-Hall, 2003.
[55] X. Jin, G. Chen, J. Hou, Q. Jiang, D. Zhou, and S. Yao, "Multimodal sensor medical image fusion based on nonsubsampled shearlet transform and S-PCNNs in HSV space," *Signal Process.*, vol. 153, pp. 379–395, Dec. 2018.

YO-PING HUANG (Fellow, IEEE) received the Ph.D. degree in electrical engineering from Texas Tech University, Lubbock, TX, USA.

He was a Professor and the Dean of the Research and Development, from 2005 to 2007, the Dean of the College of Electrical Engineering and Computer Science, from 2002 to 2005, and the Department Chair with Tatung University, Taipei, from 2000 to 2002. He is currently a Professor with the Department of Electrical Engineering, National Taipei University of Technology, Taipei, Taiwan, where he served as the Secretary General, from 2008 to 2011. His current research interests include fuzzy systems design and modeling, deep learning modeling, intelligent control, AI in agriculture, and rehabilitation systems design. He is a Fellow of IET and International Association of Grey System and Uncertain Analysis. He serves as the President of the Taiwan Association of Systems Science and Engineering, the IEEE SMCS BoG, the Chair of the IEEE SMCS Technical Committee on Intelligent Transportation Systems, and the Chair of the Taiwan SIGSPATIAL ACM Chapter. He was the Chair of the IEEE SMCS Taipei Chapter, the Chair of the IEEE CIS Taipei Chapter, and the CEO of the Joint Commission of Technological and Vocational College Admission Committee, Taiwan, from 2011 to 2015.

PRITPAL SINGH received the Ph.D. degree in computer science and engineering from Tezpur (A Central University) University, Tezpur, India, in February 2015.

He was appointed as a Faculty at the School of Mathematics and Computer Applications, Thapar University, India, in July 2013. He is currently working as a Postdoctoral Research Fellow with the Department of Electrical Engineering, National Taipei University of Technology. His research interests include power rehabilitation, image processing and segmentation, machine learning, optimization algorithm, soft computing, data analysis, and mathematical modeling and simulation. He has published numerous articles in refereed journals, conference proceedings, book chapters, and book. He received the Postdoctoral Research Fellowship from the Ministry of Science and Technology (MOST), Taiwan, in March 2019. His research articles can be found in *Knowledge and Information Systems* (Springer), *Knowledge-Based Systems* (Elsevier), *International Journal of Approximate Reasoning* (Elsevier), *Engineering Applications of Artificial Intelligence* (Elsevier), *International Journal of Machine Learning and Cybernetics* (Springer), *Stochastic Environmental Research and Risk Assessment* (Springer), *Applied Soft Computing* (Elsevier), *Journal of Computational Science* (Elsevier), and *Computers in Industry* (Elsevier), among others.

HUNG-CHOU KUO graduated from National Taiwan University, Taipei, and Kaohsiung Medical University, Kaohsiung, Taiwan.

He is currently an Associated Professor and the Director of the Section of Neuromuscular Disease, Department of Neurology, Chang Gung Memorial Hospital and Linkou Medical Center, University Medical College, Taoyuan, Taiwan. He has authored more than 110 articles and three book chapters. His research interests include neuromuscular disorders, hepatic porphyria, dementia, nervous system infection, electrophysiology in neurology, and neurotoxicology. His current research is focusing in metabolomics for diabetic polyneuropathy, Alzheimer's disease, acute intermittent porphyria, and amyotrophic lateral sclerosis.